Available online at www.sciencedirect.com

ScienceDirect

Advances in Space Research 74 (2024) 4368–4376

ADVANCES IN SPACE RESEARCH (a COSPAR publication)

www.elsevier.com/locate/asr

Direct measurements of cosmic – Ray iron and nickel with CALET on the International Space Station

O. Adriani [a,b], Y. Akaike [c,d], K. Asano [e], Y. Asaoka [e], E. Berti [b], G. Bigongiari [f,g], W.R. Binns [h], M. Bongi [a,b], P. Brogi [f,g], A. Bruno [i], N. Cannady [j,k,l], G. Castellini [m], C. Checchia [f,g,*], M.L. Cherry [n], G. Collazuol [o,p], G.A. de Nolfo [i], K. Ebisawa [q], A.W. Ficklin [n], H. Fuke [q], S. Gonzi [a,b], T.G. Guzik [n], T. Hams [j], K. Hibino [r], M. Ichimura [s], K. Ioka [t], W. Ishizaki [e], M.H. Israel [h], K. Kasahara [u], J. Kataoka [v], R. Kataoka [w], Y. Katayose [x], C. Kato [y], N. Kawanaka [t,z], Y. Kawakubo [n], K. Kobayashi [c,d], K. Kohri [aa], H.S. Krawczynski [h], J.F. Krizmanic [k], P. Maestro [f,g], P.S. Marrocchesi [f,g], M. Mattiazzi [f,p], A.M. Messineo [ab,g], J.W. Mitchell [k], S. Miyake [ac], A.A. Moiseev [ad,k,l], M. Mori [ae], N. Mori [b], H.M. Motz [c], K. Munakata [y], S. Nakahira [q], J. Nishimura [q], S. Okuno [r], J.F. Ormes [af], S. Ozawa [ag], L. Pacini [b,m], P. Papini [b], B.F. Rauch [h], S.B. Ricciarini [m,b], K. Sakai [j,k,l], T. Sakamoto [ah], M. Sasaki [ad,k,l], Y. Shimizu [r], A. Shiomi [ai], P. Spillantini [a], F. Stolzi [f,g], S. Sugita [ah], A. Sulaj [f,g], M. Takita [e], T. Tamura [r], T. Terasawa [e], S. Torii [c], Y. Tsunesada [aj,ak], Y. Uchihori [al], E. Vannuccini [b], J.P. Wefel [n], K. Yamaoka [am], S. Yanagita [an], A. Yoshida [ah], K. Yoshida [u], W.V. Zober [h]

[a] *Department of Physics, University of Florence, Via Sansone, 1, 50019 Sesto Fiorentino, Italy*
[b] *INFN Sezione di Florence, Via Sansone, 1 - 50019, Sesto Fiorentino, Italy*
[c] *Waseda Research Institute for Science and Engineering, Waseda University, 17 Kikuicho, Shinjuku, Tokyo 162-0044, Japan*
[d] *JEM Utilization Center, Human Spaceflight Technology Directorate, Japan Aerospace Exploration Agency, 2-1-1 Sengen, Tsukuba, Ibaraki 305-8505, Japan*
[e] *Institute for Cosmic Ray Research, The University of Tokyo, 5-1-5 Kashiwa-no-Ha, Kashiwa, Chiba 277-8582, Japan*
[f] *Department of Physical Sciences, Earth and Environment, University of Siena, Via Roma 56, 53100 Siena, Italy*
[g] *INFN Sezione di Pisa, Polo Fibonacci, Largo B. Pontecorvo, 3, 56127 Pisa, Italy*
[h] *Department of Physics and McDonnell Center for the Space Sciences, Washington University, One Brookings Drive, St. Louis, MS 63130-4899, USA*
[i] *Heliospheric Physics Laboratory, NASA/GSFC, Greenbelt, MD 20771, USA*
[j] *Center for Space Sciences and Technology, University of Maryland, Baltimore County, 1000 Hilltop Circle, Baltimore, MD 21250, USA*
[k] *Astroparticle Physics Laboratory, NASA/GSFC, Greenbelt, MD 20771, USA*
[l] *Center for Research and Exploration in Space Sciences and Technology, NASA/GSFC, Greenbelt, MD 20771, USA*
[m] *Institute of Applied Physics (IFAC), National Research Council (CNR), Via Madonna del Piano, 10, 50019, Sesto Fiorentino, Italy*
[n] *Department of Physics and Astronomy, Louisiana State University, 202 Nicholson Hall, Baton Rouge, LA 70803, USA*
[o] *Department of Physics and Astronomy, University of Padova, Via Marzolo, 8, 35131 Padova, Italy*
[p] *INFN Sezione di Padova, Via Marzolo, 8, 35131 Padova, Italy*
[q] *Institute of Space and Astronautical Science, Japan Aerospace Exploration Agency, 3-1-1 Yoshinodai, Chuo, Sagamihara, Kanagawa 252-5210, Japan*
[r] *Kanagawa University, 3-27-1 Rokkakubashi, Kanagawa, Yokohama, Kanagawa 221-8686, Japan*
[s] *Faculty of Science and Technology, Graduate School of Science and Technology, Hirosaki University, 3, Bunkyo, Hirosaki, Aomori 036-8561, Japan*
[t] *Yukawa Institute for Theoretical Physics, Kyoto University, Kitashirakawa Oiwake-cho, Sakyo-ku, Kyoto, 606-8502, Japan*
[u] *Department of Electronic Information Systems, Shibaura Institute of Technology, 307 Fukasaku, Minuma, Saitama 337-8570, Japan*

* Corresponding author at: Department of Physical Sciences, Earth and Environment, University of Siena, via Roma 56, 53100 Siena, Italy.
E-mail address: caterina.checchia2@unisi.it (C. Checchia), .

https://doi.org/10.1016/j.asr.2024.03.052
0273-1177/

[v] School of Advanced Science and Engineering, Waseda University, 3-4-1 Okubo, Shinjuku, Tokyo 169-8555, Japan
[w] National Institute of Polar Research, 10-3, Midori-cho, Tachikawa, Tokyo 190-8518, Japan
[x] Faculty of Engineering, Division of Intelligent Systems Engineering, Yokohama National University, 79-5 Tokiwadai, Hodogaya, Yokohama 240-8501, Japan
[y] Faculty of Science, Shinshu University, 3-1-1 Asahi, Matsumoto, Nagano 390-8621, Japan
[z] Department of Astronomy, Graduate School of Science, Kyoto University, Kitashirakawa Oiwake-cho, Sakyo-ku, Kyoto, 606-8502, Japan
[aa] Institute of Particle and Nuclear Studies, High Energy Accelerator Research Organization, 1-1 Oho, Tsukuba, Ibaraki 305-0801, Japan
[ab] University of Pisa, Polo Fibonacci, Largo B. Pontecorvo, 3 - 56127 Pisa, Italy
[ac] Department of Electrical and Electronic Systems Engineering, National Institute of Technology, Ibaraki College, 866 Nakane, Hitachinaka, Ibaraki 312-8508, Japan
[ad] Department of Astronomy, University of Maryland, College Park, MD 20742, USA
[ae] Department of Physical Sciences, College of Science and Engineering, Ritsumeikan University, Shiga 525-8577, Japan
[af] Department of Physics and Astronomy, University of Denver, Physics Building, Room 211, 2112 East Wesley Avenue, Denver, CO 80208-6900, USA
[ag] Quantum ICT Advanced Development Center, National Institute of Information and Communications Technology, 4-2-1 Nukui-Kitamachi, Koganei, Tokyo 184-8795, Japan
[ah] College of Science and Engineering, Department of Physics and Mathematics, Aoyama Gakuin University, 5-10-1 Fuchinobe, Chuo, Sagamihara, Kanagawa 252-5258, Japan
[ai] College of Industrial Technology, Nihon University, 1-2-1 Izumi, Narashino, Chiba 275-8575, Japan
[aj] Division of Mathematics and Physics, Graduate School of Science, Osaka Metropolitan University, 3-3-138 Sugimoto, Sumiyoshi, Osaka 558-8585, Japan
[ak] Nambu Yoichiro Institute of Theoretical and Experimental Physics, Osaka Metropolitan University, 3-3-138 Sugimoto, Sumiyoshi, Osaka 558-8585, Japan
[al] National Institutes for Quantum and Radiation Science and Technology, 4-9-1 Anagawa, Inage, Chiba 263-8555, Japan
[am] Nagoya University, Furo, Chikusa, Nagoya 464-8601, Japan
[an] College of Science, Ibaraki University, 2-1-1 Bunkyo, Mito, Ibaraki 310-8512, Japan

Received 10 November 2023; received in revised form 19 February 2024; accepted 22 March 2024
Available online 27 March 2024

Abstract

Iron and nickel cosmic ray nuclei play a key role in the understanding of the acceleration and propagation mechanisms of charged particles in our Galaxy. In fact, iron and nickel are the most abundant nuclei among the heavy elements and provide favorable conditions for a low background measurement thanks to the negligible contamination from spallation of higher mass elements. CALET, operating on the ISS since 2015, has excellent capabilities of charge discrimination up to nickel and can measure the energy of cosmic ray nuclei thanks to a lead tungstate calorimeter providing a direct and precise measurement of heavy charged nuclei spectra. In this contribution, a direct measurement of iron and nickel nuclei spectra in the energy range from 10 GeV/n to 2 TeV/n and from 8.8 GeV/n to 240 GeV/n, respectively is presented. More than five years of data collected by CALET were used. A detailed study of systematic uncertainties is also illustrated. The measured spectra are compared with the ones measured by other experiments and are compatible with a single power law fit in the energy region from 50 GeV/n to 2 TeV/n and from 20 GeV/n to 240 GeV/n for iron and nickel respectively. Also, the ratio between nickel and iron spectra is reported.

Keywords: Astroparticle; Cosmic-rays; Iron spectrum; Nickel spectrum

1. Introduction

The acceleration and propagation mechanisms of charged particles in our Galaxy can be theoretically understood through key observables such as energy spectra and relative abundances of cosmic rays (CR) (Blasi et al., 2012; Tomassetti, 2012; Evoli et al., 2018; Vladimirov et al., 2012; Ptuskin et al., 2013; Thoudam and Hörandel, 2014; Drury, 2011; Bernard et al., 2013; Serpico, 2016; Ohira et al., 2016; Caprioli et al., 2021; Lipari, 2021). Direct measurements from space-based instruments and ballon-borne calorimeters together with indirect measurements from ground-based arrays revealed a progressive hardening of proton and He spectra at a few hundred GeV/n (Aguilar et al., 2015a; Aguilar et al., 2015b; Adriani et al., 2011; Yoon et al., 2011; Yoon et al., 2017; An et al., 2019; Adriani et al., 2019; Adriani et al., 2023) which has also been observed for heavier nuclei (Aguilar et al., 2017; Aguilar et al., 2018; Aguilar et al., 2020; Ahn et al., 2010; Adriani et al., 2020). Also, a spectral softening has been observed for proton and helium spectra in the TeV region, as reported by the DAMPE (An et al., 2019; Alemanno et al., 2021), CALET (Adriani et al., 2022a, 2023) and NUCLEON (Grebenyuk et al., 2019) experiments. The accurate investigation of heavy cosmic ray nuclei spectra and their ratios is of great interest in order to discriminate among different interpretations of the propagation and the acceleration phenomena in our Galaxy. In this context, the iron and nickel nuclei provide favorable conditions for observation because they are the most abundant among

the heavy elements and they are scarcely affected by the spallation contamination from higher mass elements.

The most recent measurement of the iron spectrum is provided by the spectrometer AMS-02 (Aguilar et al., 2021) preceded by other direct measurements from satellites (Engelmann et al., 1990; Mueller et al., 1991; Grebenyuk et al., 2019) and balloons (Ichimura et al., 1993; Panov et al., 2009; Obermeier et al., 2011; Ave et al., 2008; Ahn et al., 2009). For the nickel spectrum few direct measurements (Engelmann et al., 1990; Grebenyuk et al., 2018) are available and most of them are limited to a few tens of GeV/n (Lave et al., 2013, 2016, 1974, 1981, 1978, 1981, 1992).

CALET in orbit on the International Space Station (Marrocchesi and Torii, 2019; Marrocchesi, 2021) is a space-based instrument optimized to detect the all-electron spectrum (Adriani et al., 2017; Adriani et al., 2018) but also able to distinguish between each nuclear species up to nickel and above, providing spectra up to the PeV scale. This can be achieved thanks to its large dynamic range, adequate calorimeter depth, accurate tracking and excellent charge identification capabilities. CALET was launched in August 19, 2015 and it is now installed on the Japanese Exposure Facility of the International Space Station. During the first weeks after launch the on-orbit commissioning phase was successfully completed. The detector has been collecting scientific data since October 13, 2015.

In this paper, we present a summary of the differential energy spectrum of CR iron and nickel nuclei with CALET from 10 GeV/n to 2.2 TeV/n and from 8.8 GeV/n and 240 GeV/n respectively, based on our previous publications (Adriani et al., 2021; Adriani et al., 2022b).

2. The CALET instrument

The CALET instrument is composed of three subdetectors each one with a specific task: the CHarge Detector is a two-layered hodoscope of plastic scintillator paddles designated to accurately measure the charge of incident particles up to nickel and above (up $Z = 40$) with excellent charge resolution ranging from 0.15 e (charge units) for C to 0.39 e for Ni. The IMC (IMaging Calorimeter) is a pre-shower calorimeter (3 radiation lengths, 0.1 proton interaction lengths) equipped with 16 layers of thin scintillating fiber arranged in belts along orthogonal directions and interleaved with tungsten absorbers able to reconstruct the particle trajectory. It can also provide an independent charge measurement via multiple samples of specific energy loss (dE/dx) in each fiber up to the onset of saturation which occurs for nuclei with Z >14. Therefore, the iron and nickel nuclei identification relies on CHD only. The energy of incident particles is measured by the Total Absorption Calorimeter (TASC), a homogeneous calorimeter made of lead-tungstate bars arranged in 12 layers, covering 27 radiation lengths (1.2 proton interaction lengths). The crystal bars in the top layer are read out by photomultiplier tubes, while a dual photodiode–ava lanche-photodiode (PD–APD) system is used for each channel in the remaining layers. The field of view of CALET is $\sim 45°$from zenith. More details on the instrument can be found in the Supplemental Material of Adriani et al. (2017).

3. Data analysis

The analyses here reported cover a period of 1613 days for iron and 2038 days for nickel with a total observation live time for high energy (HE) shower trigger (Asaoka et al., 2017) $T \sim 3.3 \times 10^4$ h and $T \sim 4.1 \times 10^4$ h respectively, corresponding to 86% of total observation time. The calibration of each channel of CHD, IMC and TASC is performed using penetrating protons and He particles, selected in-flight with a dedicated trigger mode (Asaoka et al., 2017; Niita et al., 2015). Raw data are corrected for gain differences among the channels, light output nonuniformity, and any residual dependence on time and temperature. After calibration, a "best track" is reconstructed for each CR particle with an associated estimate of its charge and energy. A combinatorial Kalman filter algorithm fed with the coordinates provided by the IMC fibers, is used for tracking and provides the particle trajectory and the entrance point. The angular resolution and the spatial resolution for the impact point on the CHD are $\sim 0.08°$ and $\sim 180\,\mu$m, respectively both for iron and nickel.

Monte Carlo (MC) simulations, reproducing the detailed detector configuration, physical processes, as well as detector signals are based on the EPICS simulation package (Kasahara, 1995). Independent simulations based on FLUKA (Böhlen et al., 2014) and GEANT4 (Allison et al., 2016) are used to assess the systematic uncertainties for iron and nickel, respectively.

3.1. Charge reconstruction

The identification of the particle's charge Z is based on the measurement of the ionization deposits in the CHD paddles traversed by the incident particle and properly corrected for its path length. Each CHD layer provides an independent dE/dx measurement. The quenching effect in the scintillator's light yield is corrected for by fitting the dE/dx as a function of Z^2 to a "halo" model (Marrocchesi et al., 2011). The resulting curves are used to reconstruct a charge value in either layer on an event-by-event basis (Adriani et al., 2020). The charge identification is affected by the presence of backscattering particles from the TASC, more important at higher energies. The observed effect is the generation of additional energy deposits in the CHD, which enhance the primary particle ionization signal. As a consequence, the charge peaks of CHDx and CHDy exhibit a systematic shift towards higher values, up to 0.8 charge units, when compared to their

nominal position. Therefore, the peak positions of iron, nickel and the neighbour elements are restored to their nominal values by an energy dependent charge correction applied separately to the FD and the MC data. The CHD charge resolution is determined by the distribution of the average charge between CHDx and CHDy and amounts to 0.35 and 0.39 charge units for iron and nickel respectively.

3.2. Energy measurement

The TASC logs have two independent light readout, one with a larger area avalanche photodiode and the other with a smaller area photodiode. The total dynamic range (from 1 MiP to 10^6 MiP) is split into four sub-ranges using a double-gain shaper amplifier. The shower energy E_{TASC} is calculated as the sum of the energy deposits in all TASC logs after stitching the adjacent gain ranges of each PD-APD (Asaoka et al., 2017).

The TASC response to nuclei was studied at CERN SPS in 2015 using a beam of accelerated ion fragments with A/Z = 2 and kinetic energy of 13, 19 and 150 GeV/c/n. The resulting energy distribution looks nearly gaussian, the energy released in the TASC is ~20% of the particle energy and the resolution is close to 30%. The energy response of TASC is linear up to the maximum available particle energy of 6 TeV. The energy response derived from MC simulations was tuned using the beam test results. Correction factors are 6.7% for $E_{TASC} < 45$ GeV and 3.5% for $E_{TASC} > 350$ GeV, respectively, while a simple linear interpolation is used to determine the correction factor for intermediate energies.

3.3. Event selection

A fiducial volume based on events whose reconstructed track crosses the detector from the top of the CHD to the bottom of the TASC and clear from the edges of the top and bottom TASC layers is applied for iron events. No condition on TASC bottom layer is requested in the nickel analysis. The resulting geometrical factors are $S\Omega \sim 416$ cm^2 sr for iron and $S\Omega \sim 510$ cm^2 sr for nickel in order to increase the statistics.

The particles undergoing a charge-changing nuclear interaction in the upper part of the instrument are removed by requiring that the difference between the CHDX and CHDY charge is less than 1.5 charge units. Since the HE trigger, based on the coincidence of the summed signals of the last four IMC layers and the top TASC layer, is fully efficient for elements heavier than oxygen, an off-line trigger confirmation, as required for the analysis of lower charge elements (Adriani et al., 2020; Adriani et al., 2022a; Adriani et al., 2022c) is not necessary for these analyses. However, a shower event cut based on events whose deposit in at least one of the first four layers of TASC is larger by 2 sigmas than the minimum ionization (MI) particle peak, is applied in order to select interacting particles. Iron (nickel) candidates are selected in the CHDX - CHDY plane using an ellipse centered on the nominal charge values Z = 26 (28) with 1.25 (1.4) σ_x and 1.25 (1.4) σ_y wide semi-axes for Z_{CHDX} and Z_{CHDY}, respectively, and rotated clockwise by 45° as shown in Fig. 1. Following the aforementioned cuts, 5.2×10^3 Ni and 4.1×10^4 Fe candidate events are identified.

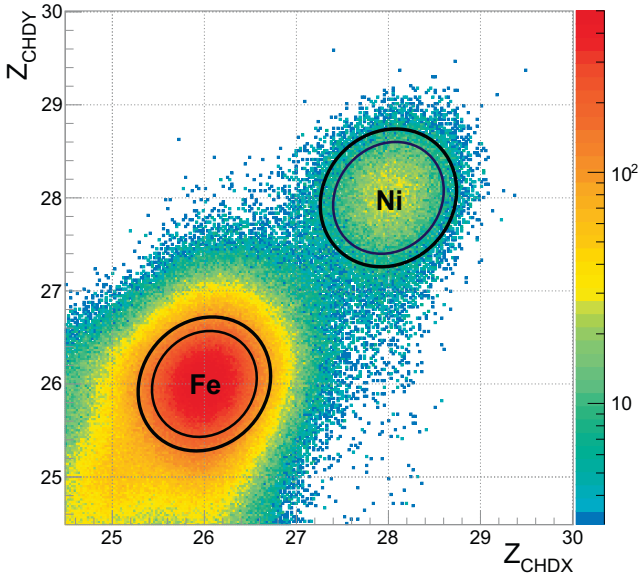

Fig. 1. Crossplot of Z_{CHDX} vs Z_{CHDY} reconstructed charges in the elemental range between Mn (Z = 25) and Zn (Z = 30). The ellipses indicate the maximum and minimum charge selection (depending on the energy) for iron and nickel.

For the flux measurement, energy unfolding is applied to correct E_{TASC} distributions of selected Fe and Ni candidates for significant bin-to-bin migration effects (due to the limited energy resolution) and infer the primary particle energy. In these analyses we used a Bayesian approach implemented within the RooUnfold package of the ROOT analysis framework. Each element of the response matrix represents the probability that a primary nucleus in a given energy interval of cosmic ray spectrum produces an energy deposit into a given bin of E_{TASC}. The response matrices are produced from the MC simulations after applying the same selection criteria as for FD. More details can be found in the supplemental material of Adriani et al. (2021, 2022b).

3.4. Differential energy spectra

The energy spectrum is obtained from the unfolded energy distribution as follows:

$$\Phi(E) = \frac{N(E)}{\Delta E\, \varepsilon(E)\, S\Omega\, T} \quad (1)$$

$$N(E) = U[N_{obs}(E_{TASC}) - N_{bg}(E_{TASC})] \quad (2)$$

where $S\Omega$ and T are the geometrical factor and the live time respectively, ΔE denotes the energy bin width, E is the geo-

metric mean of the lower and upper bounds of the bin, $N(E)$ is the bin content in the unfolded distribution, $\varepsilon(E)$ is the total selection efficiency (Adriani et al., 2021; Adriani et al., 2022b), $U()$ is the unfolding procedure operator, $N_{obs}(E_{TASC})$ is the bin content of observed energy distribution (including background), and $N_{bg}(E_{TASC})$ is the bin content of background events in the observed energy distribution. The most important source of background contamination is given by different nuclear species misidentified as Fe or Ni. It was estimated to be $< 1\%$ in the energy range between 10^2 and 10^3 GeV of E_{TASC} increasing up to $\sim 2\%$ at $E_{TASC} \sim 10^4$ GeV for iron. Background contamination for Ni is similar to that of Fe up to 10^3 GeV and it increases up to 10% at $\sim 10^4$ GeV.

4. Systematic errors

An accurate study of systematic uncertainties was carried out for these analyses. The most important systematic errors are given by the charge identification and the MC model. In order to assess the systematics due to the charge identification, the charge selection was varied changing the semi-major and minor axes of the ellipses by 15%. The resulting difference in the flux depends on the energy and it is lower than 4% for nickel below 100 GeV/n and lower than a few percent for iron below 600 GeV/n. At the highest energy, where test beam data are not available to validate the simulations, the systematic errors are estimated by using different MC models (i.e. EPICS and FLUKA for iron and EPICS and GEANT4 for nickel) and calculating the differences in the flux arising from the use of the different transport models. The total selection efficiencies for Fe and Ni determined with the two pairs of models are in agreement within few percent over the whole energy range (Adriani et al., 2021; Adriani et al., 2022b). However, the response matrices obtained with the different simulation packages differ by more than 5% in the low and high energy regions giving origin to a flux with a maximum discrepancy of 10% below 40 GeV/n (for Fe) and 10% between 100 GeV/n and 200 GeV/n (for Ni). The uncertainty on the energy scale ($\pm 2\%$) causes a rigid shift of the measured energy, converting in a different flux normalization by $^{+3.3\%}_{-3.2\%}$ for Fe and $\pm 4\%$ for Ni without affecting the spectral shape. Different response matrices computed by varying the spectral index (between -2.9 and -2.2) were used to assess the systematics due to the unfolding procedure. Also, the differences in the beam test model with respect to the instrument now in flight causes a difference in the final spectra that was modeled and included in the systematic uncertainty. The resulting difference in the flux is less than 5% at 140 GeV/n for Ni and less than 6% in the TeV region for Fe. The contribution due to a shower event cut, rejecting noninteracting particles, was evaluated and considered in the systematic uncertainties. The systematic uncertainty due to off-acceptance events, tracking efficiency, background contamination and HE trigger efficiency are negligible both for iron and nickel. The fraction of interactions in the upper part of the detector is checked by comparing the MC and the FD as explained in the Supplemental Material of Adriani et al. (2021) and Adriani et al. (2022b). In the nickel analysis only ^{58}Ni isotope was considered since its mass difference with respect to other isotopes is less than 3%. However, a systematic error related to the atomic mass of the isotope composition was considered and reduces the normalization of the flux by

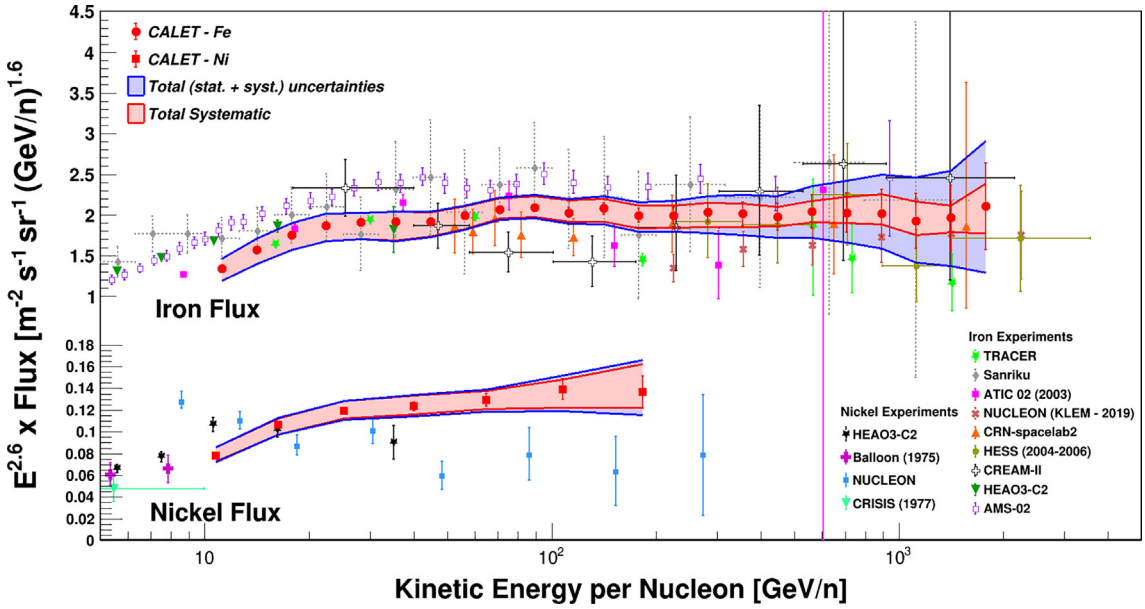

Fig. 2. CALET Fe and Ni fluxes (multiplied by $E^{2.6}$) as a function of kinetic energy per nucleon. The error bars of the CALET data (red) represent the statistical uncertainty only, the red band indicates the quadrature sum of systematic errors, while the blue band indicates the quadrature sum of statistical and systematic errors. Also plotted are other direct measurements. (For interpretation of the references to colour in this figure legend, the reader is referred to the web version of this article.)

2%. Additional energy independent contributions affecting the normalization of the flux but not the spectral shape are given by the live time (3.4%), long term stability (<2%), geometrical factor (~ 1.6%). Finally, the total systematic uncertainty is computed as the quadrature sum of each contribution.

5. Results

The energy spectra of iron and nickel cosmic ray nuclei measured with CALET in the energy interval between 10 GeV/n and 2.2 TeV/n (iron) and between 8.8 GeV/n and 240 GeV/n (nickel) are reported in Fig. 2 where previous measurements are also depicted. The total systematic error band is represented by the red shaded area whereas the blue one indicates the total error calculated as the quadrature sum of systematic and statistical error (the latter shown by red bars). CALET iron result turns out to be consistent with ATIC 02 (Panov et al., 2009) and TRACER (Ave et al., 2008) at low energy and with CNR (Mueller et al., 1991) and HESS (Aharonian et al., 2007) at high energy. A discrepancy in the spectrum normalization is observed with respect to AMS-02 (Aguilar et al., 2021) (~20%) and with respect to NUCLEON

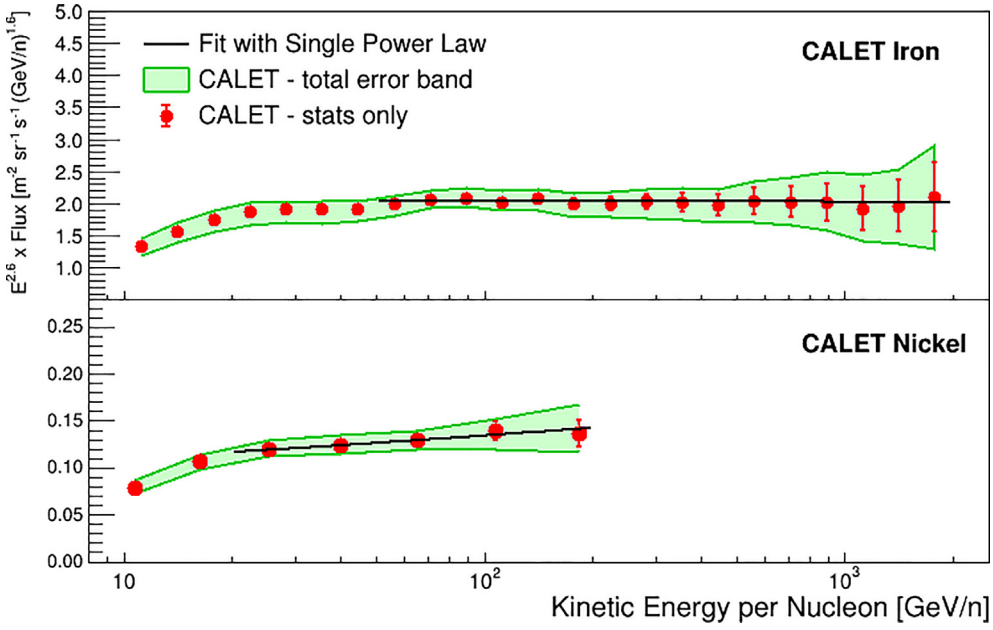

Fig. 3. Single power law fit on iron (top) and nickel (bottom) spectra. The fit (black lines) was performed from 50 GeV/n to 2 TeV/n on iron spectrum and from 20 GeV/n to 240 GeV/n on nickel spectrum. The green bands are representative of total errors whereas the red bars indicate the statistical uncertainty. The results are $\gamma_{Fe} = -2.60 \pm 0.03$ and $\gamma_{Ni} = -2.51 \pm 0.07$ for iron and nickel respectively. (For interpretation of the references to colour in this figure legend, the reader is referred to the web version of this article.)

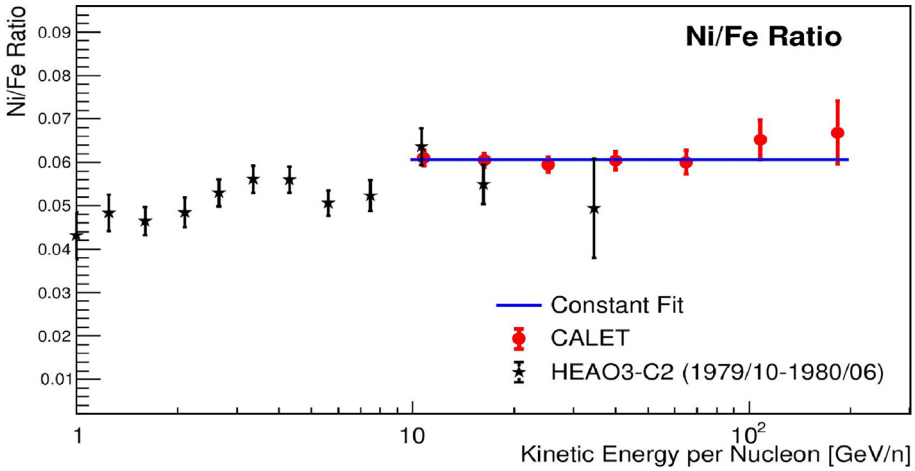

Fig. 4. The nickel to iron ratio measured by CALET between 10 GeV/n and 240 GeV/n. The measurement is compatible with the result from HEAO3-C2 in the common interval of energies. A constant fit (blue line) was performed giving a value of 0.061 ± 0.001. (For interpretation of the references to colour in this figure legend, the reader is referred to the web version of this article.)

(Grebenyuk et al., 2019) (∼14%). The nickel spectrum is in agreement with HEAO-C3 in the common interval of energies covered by both experiments. CALET and NUCLEON differ in shape although the two measurements show a similar flux normalization.

Both spectra were fitted by a single power law (SPL) to assess the spectral index. Fig. 3 reports the results for iron and nickel. The fits were performed from 50 GeV/n to 2.2 TeV/n and from 20 GeV/n to 240 GeV/n giving a spectral index $\gamma_{Fe} = -2.60 \pm 0.02\,(\text{stat}) \pm 0.02\,(\text{sys})$, with $\chi^2/dof = 4.2/14$ and $\gamma_{Ni} = -2.51 \pm 0.04\,(\text{stat}) \pm 0.06\,(\text{sys})$ with $\chi^2/dof = 0.3/3$ for iron and nickel respectively. In the energy region below 20 GeV/n the flux softening is similar for iron and nickel spectra and compatible with the one observed for lighter nuclei.

The nickel to iron ratio is reported in Fig. 4 extending the previous measurement obtained by HEAO3-C2 (Engelmann et al., 1990) up to 240 GeV/n. The trend is compatible with a constant of value 0.061 ± 0.001(stat.) with a $\chi^2/dof = 2.6/6$. This indicates that the energy dependence of iron and nickel spectra is similar and suggests that their acceleration and propagation behaviour might be the same.

6. Conclusions

A measurement of the energy spectra of iron and nickel from 10 GeV/n to 2.0 TeV/n and from 8.8 to 240 GeV/n, respectively was reported enhancing the precision of most of the existing measurements. Between 50 (20) GeV/n and 2000 (240) GeV/n the Fe (Ni) spectrum is consistent with the hypothesis of a SPL with a spectral index $\gamma_{Fe} = -2.60 \pm 0.03$ $(\gamma_{Ni} = -2.51 \pm 0.07)$. The present statistics and the large systematic errors at high energy do not allow us to draw a significant conclusion on a possible deviation from a single power law. We expect that the enhancement in the statistics beyond the current period of 53 months (for iron) and 67 months (for nickel), will improve our measurements reducing the statistical and systematic uncertainties. For iron in particular, the reduction of the uncertainties will give us the possibility to test hypotheses different from a single power law.

The flat behavior of the nickel to iron ratio suggests that both elements have very similar fluxes in shape and energy dependence, suggesting that their origin, acceleration, and propagation might be explained by invoking an identical mechanism in the explored energy range.

Declaration of Competing Interest

The authors declare that they have no known competing financial interests or personal relationships that could have appeared to influence the work reported in this paper.

Acknowledgments

We gratefully acknowledge JAXA's contribution to the development of the CALET project and to the operations onboard the ISS. We also wish to express our sincere gratitude to ASI and NASA for their support to the CALET mission. CALET project is supported in part by JAXA through JSPS KAKENHI Grants No. 19H05608, No. 17H02901, No. 21K03592, and No. 21K03604 and by the MEXT-Supported Program for the Strategic Research Foundation at Private Universities (2011–2015) (No. S1101021) at Waseda University. The CALET effort in Italy is supported by ASI under Agreement No. 2013–018-R.0 and its amendments and in USA by NASA through Grants No. 80NSSC20K0397, No. 80NSSC20K0399, and No. NNH18ZDA001N-APRA18-0004.

References

Adriani, O., Akaike, Y., Asano, K., et al.CALET Collaboration, 2019. Direct measurement of the cosmic-ray proton spectrum from 50 gev to 10 tev with the calorimetric electron telescope on the international space station. Phys. Rev. Lett. 122, 181102. https://doi.org/10.1103/PhysRevLett.122.181102, URL: https://link.aps.org/doi/10.1103/PhysRevLett.122.181102.

Adriani, O., Akaike, Y., Asano, K., et al.CALET Collaboration, 2018. Extended Measurement of the Cosmic-Ray Electron and Positron Spectrum from 11 GeV to 4.8 TeV with the Calorimetric Electron Telescope on the International Space Station. Phys. Rev. Lett. 120, 261102. https://doi.org/10.1103/PhysRevLett.120.261102, URL: https://link.aps.org/doi/10.1103/PhysRevLett.120.261102.

Adriani, O., Akaike, Y., Asano, K., et al.CALET Collaboration, 2020. Direct Measurement of the Cosmic-Ray Carbon and Oxygen Spectra from 10 GeV/n to 2.2 TeV/n with the Calorimetric Electron Telescope on the International Space Station. Phys. Rev. Lett. 125, 251102. https://doi.org/10.1103/PhysRevLett.125.251102, URL: https://link.aps.org/doi/10.1103/PhysRevLett.125.251102.

Adriani, O., Akaike, Y., Asano, K., et al.CALET Collaboration, 2017. Energy Spectrum of Cosmic-Ray Electron and Positron from 10 GeV to 3 TeV Observed with the Calorimetric Electron Telescope on the International Space Station. Phys. Rev. Lett. 119, 181101. https://doi.org/10.1103/PhysRevLett.119.181101, URL: https://link.aps.org/doi/10.1103/PhysRevLett.119.181101.

Adriani, O., Akaike, Y., Asano, K., et al.CALET Collaboration, 2022a. Observation of spectral structures in the flux of cosmic-ray protons from 50 gev to 60 tev with the calorimetric electron telescope on the international space station. Phys. Rev. Lett. 129, 101102. https://doi.org/10.1103/PhysRevLett.129.101102, URL: https://link.aps.org/doi/10.1103/PhysRevLett.129.101102.

Adriani, O., Akaike, Y., Asano, K., et al.CALET Collaboration, 2022b. Direct measurement of the nickel spectrum in cosmic rays in the energy range from 8.8 GeV/n to 240 GeV/n with calet on the international space station. Phys. Rev. Lett. 128, 131103. https://doi.org/10.1103/PhysRevLett.128.131103, URL: https://link.aps.org/doi/10.1103/PhysRevLett.128.131103.

Adriani, O., Akaike, Y., Asano, K., et al.CALET Collaboration, 2021. Measurement of the iron spectrum in cosmic rays from 10 GeV/n to 2.0 TeV/n with the calorimetric electron telescope on the international space station. Phys. Rev. Lett. 126, 241101. https://doi.org/10.1103/PhysRevLett.126.241101, URL: https://link.aps.org/doi/10.1103/PhysRevLett.126.241101.

Adriani, O., Akaike, Y., Asano, K., et al.CALET Collaboration, 2023. Direct measurement of the cosmic-ray helium spectrum from 40 gev to

250 tev with the calorimetric electron telescope on the international space station. Phys. Rev. Lett. 130, 171002. https://doi.org/10.1103/PhysRevLett.130.171002, URL: https://link.aps.org/doi/10.1103/PhysRevLett.130.171002.

Adriani, O., Akaike, Y., Asano, K., et al.CALET Collaboration, 2022c. Cosmic-ray boron flux measured from 8.4 GeV/n to 3.8 TeV/n with the calorimetric electron telescope on the international space station. Phys. Rev. Lett. 129, 251103. https://doi.org/10.1103/PhysRevLett.129.251103, URL: https://link.aps.org/doi/10.1103/PhysRevLett.129.251103.

Adriani, O., Barbarino, G.C., Bazilevskaya, G.A. et al., 2011. PAMELA Measurements of Cosmic-Ray Proton and Helium Spectra. Science, 332(6025), 69–72. URL: https://www.science.org/doi/abs/10.1126/science.1199172. doi:10.1126/science.1199172. arXiv:https://www.science.org/doi/pdf/10.1126/science.1199172.

Aguilar, M., Aisa, D., Alpat, B., et al.AMS Collaboration, 2015a. Precision Measurement of the Proton Flux in Primary Cosmic Rays from Rigidity 1 GV to 1.8 TV with the Alpha Magnetic Spectrometer on the International Space Station. Phys. Rev. Lett. 114, 171103. https://doi.org/10.1103/PhysRevLett.114.171103, URL: https://link.aps.org/doi/10.1103/PhysRevLett.114.171103.

Aguilar, M., Aisa, D., Alpat, B., et al.AMS Collaboration, 2015b. Precision Measurement of the Helium Flux in Primary Cosmic Rays of Rigidities 1.9 GV to 3 TV with the Alpha Magnetic Spectrometer on the International Space Station. Phys. Rev. Lett. 115, 211101. https://doi.org/10.1103/PhysRevLett.115.211101, URL: https://link.aps.org/-doi/10.1103/PhysRevLett.115.211101.

Aguilar, M., Ali Cavasonza, L., Alpat, B., et al.AMS Collaboration, 2017. Observation of the identical rigidity dependence of He, C, and O cosmic rays at high rigidities by the alpha magnetic spectrometer on the International Space Station. Phys. Rev. Lett. 119, 251101. https://doi.org/10.1103/PhysRevLett.119.251101, URL: https://link.aps.org/-doi/10.1103/PhysRevLett.119.251101.

Aguilar, M., Ali Cavasonza, L., Ambrosi, G., et al.AMS Collaboration, 2018. Observation of new properties of secondary cosmic rays lithium, beryllium, and boron by the alpha magnetic spectrometer on the International Space Station. Phys. Rev. Lett. 120, 021101. https://doi.org/10.1103/PhysRevLett.120.021101, URL: https://link.aps.org/doi/10.1103/PhysRevLett.120.021101.

Aguilar, M., Ali Cavasonza, L., Ambrosi, G., et al.AMS Collaboration, 2020. Properties of neon, magnesium, and silicon primary cosmic rays results from the alpha magnetic spectrometer. Phys. Rev. Lett. 124, 211102. https://doi.org/10.1103/PhysRevLett.124.211102, URL: https://link.aps.org/doi/10.1103/PhysRevLett.124.211102.

Aguilar, M., Cavasonza, L.A., Allen, M.S., et al.AMS Collaboration, 2021. Properties of iron primary cosmic rays: results from the alpha magnetic spectrometer. Phys. Rev. Lett. 126, 041104. https://doi.org/10.1103/PhysRevLett.126.041104, URL: https://link.aps.org/doi/10.1103/PhysRevLett.126.041104.

Aharonian, F., Akhperjanian, A.G., Bazer-Bachi, A.R., et al., 2007. First ground-based measurement of atmospheric cherenkov light from cosmic rays. Phys. Rev. D 75, 042004. https://doi.org/10.1103/PhysRevD.75.042004, URL: https://link.aps.org/doi/10.1103/PhysRevD.75.042004.

Ahn, H.S., Allison, P., Bagliesi, M.G., et al., 2009. Energy spectra of cosmic-ray nuclei at high energies. Astrophys. J. 707 (1), 593. https://doi.org/10.1088/0004-637X/707/1/593.

Ahn, H.S., Allison, P., Bagliesi, M.G., et al., 2010. Discrepant hardening observed in cosmic-ray elemental spectra. Astrophys. J. Lett. 714 (1), L89. https://doi.org/10.1088/2041-8205/714/1/L89.

Alemanno, F., An, Q., Azzarello, P., et al.DAMPE Collaboration, 2021. Measurement of the cosmic ray helium energy spectrum from 70 GeV to 80 TeV with the DAMPE Space Mission. Phys. Rev. Lett. 126, 201102. https://doi.org/10.1103/PhysRevLett.126.201102, URL: https://link.aps.org/doi/10.1103/PhysRevLett.126.201102.

Allison, J., Amako, K., Apostolakis, J., et al., 2016. Recent developments in geant4. Nucl. Instrum. Methods Phys. Res., Sect. A 835, 186–225. https://doi.org/10.1016/j.nima.2016.06.125, URL: https://www.sciencedirect.com/science/article/pii/S0168900216306957.

An, Q., Asfandiyarov, R., Azzarello, P. et al., 2019. Measurement of the cosmic ray proton spectrum from 40 GeV to 100 TeV with the DAMPE satellite. Sci. Adv., 5(9), eaax3793. URL: https://www.science.org/doi/abs/10.1126/sciadv.aax3793. doi:10.1126/sciadv.aax3793. arXiv:https://www.science.org/doi/pdf/10.1126/sciadv.aax3793.

Asaoka, Y., Akaike, Y., Komiya, Y., et al., 2017. Energy calibration of calet onboard the international space station. Astropart. Phys. 91, 1–10. https://doi.org/10.1016/j.astropartphys.2017.03.002, URL: https://www.sciencedirect.com/science/article/pii/S0927650517300786.

Ave, M., Boyle, P.J., Gahbauer, F., et al., 2008. Composition of primary cosmic-ray nuclei at high energies. Astrophys. J. 678 (1), 262. https://doi.org/10.1086/529424.

Bernard, G., Delahaye, T., Keum, Y.-Y., et al., 2013. Tev cosmic-ray proton and helium spectra in the myriad model. A&A 555, A48. https://doi.org/10.1051/0004-6361/201321202.

Blasi, P., Amato, E., Serpico, P.D., 2012. Spectral breaks as a signature of cosmic ray induced turbulence in the galaxy. Phys. Rev. Lett. 109, 061101. https://doi.org/10.1103/PhysRevLett.109.061101, URL: https://link.aps.org/doi/10.1103/PhysRevLett.109.061101.

Böhlen, T., Cerutti, F., Chin, M., et al., 2014. The FLUKA code: developments and challenges for high energy and medical applications. Nucl. Data Sheets 120, 211–214. https://doi.org/10.1016/j.nds.2014.07.049, URL: https://www.sciencedirect.com/science/article/pii/S0090375214005018.

Caprioli, D., Haggerty, C., Blasi, P., 2021. The theory of efficient particle acceleration at shocks. PoS ICRC2021, 482. https://doi.org/10.22323/1.395.0482.

Cummings, A.C., Stone, E.C., Heikkila, B.C., et al., 2016. Galactic cosmic rays in the local interstellar medium: Voyager 1 observations and model results. Astrophys. J. 831 (1), 18. https://doi.org/10.3847/0004-637X/831/1/18.

Drury, L.O., 2011. Escaping the accelerator: how, when and in what numbers do cosmic rays get out of supernova remnants? Mon. Not. R. Astron. Soc. 415 (2), 1807–1814. https://doi.org/10.1111/j.1365-2966.2011.18824.x.

Engelmann, J.J., Ferrando, P., Soutoul, A., et al., 1990. Charge composition and energy spectra of cosmic-ray nuclei for elements from Be to Ni - Results from HEAO-3-C2. Astron. Astrophys. 233, 96–111, URL: https://ui.adsabs.harvard.edu/abs/1990A&A...233...96E.

Esposito, J., Christian, E., Balasubrahmanyan, V., et al., 1992. The ALICE instrument and the measured cosmic ray elemental abundances. Astropart. Phys. 1 (1), 33–45. https://doi.org/10.1016/0927-6505(92)90007-M, URL: https://www.sciencedirect.com/science/article/pii/092765059290007M.

Evoli, C., Blasi, P., Morlino, G., et al., 2018. Origin of the cosmic ray galactic halo driven by advected turbulence and self-generated waves. Phys. Rev. Lett. 121, 021102. https://doi.org/10.1103/PhysRevLett.121.021102, URL: https://link.aps.org/doi/10.1103/PhysRevLett.121.021102.

Grebenyuk, V., Karmanov, D., Kovalev, I. et al., 2018. Cosmic ray Nickel nuclei spectrum by the NUCLEON experiment. URL: https://arxiv.org/abs/1809.07285. doi:10.48550/ARXIV.1809.07285.

Grebenyuk, V., Karmanov, D., Kovalev, I., et al., 2019. Energy spectra of abundant cosmic-ray nuclei in the NUCLEON experiment. Adv. Space Res. 64 (12), 2546–2558. https://doi.org/10.1016/j.asr.2019.10.004, URL: https://www.sciencedirect.com/science/article/pii/S0273117719307379. Advances in Cosmic-Ray Astrophysics and Related Areas.

Ichimura, M., Kogawa, M., Kuramata, S., et al., 1993. Observation of heavy cosmic-ray primaries over the wide energy range from ∼100 GeV/particle to ∼100 TeV/particle: Is the celebrated "knee" actually so prominent? Phys. Rev. D 48, 1949–1975. https://doi.org/10.1103/PhysRevD.48.1949, URL: https://link.aps.org/doi/10.1103/PhysRevD.48.1949.

Juliusson, E., 1974. Charge Composition and Energy Spectra of Cosmic-Ray Nuclei at Energies above 20 GeV Per Nucleon. Astrophys J 191, 331–348. https://doi.org/10.1086/152972.

Kasahara, K., 1995. Introduction to Cosmos and some Relevance to Ultra High Energy Cosmic Ray Air Showers. In: International Cosmic Ray Conference (p. 399). volume 1 of International Cosmic Ray Conference. URL: https://ui.adsabs.harvard.edu/abs/1995ICRC....1.399K.

Lave, K.A., Wiedenbeck, M.E., Binns, W.R., et al., 2013. Galactic cosmic-ray energy spectra and composition during the 2009–2010 solar minimum period. Astrophys. J. 770 (2), 117. https://doi.org/10.1088/0004-637X/770/2/117.

Lezniak, J.A., Webber, W.R., 1978. The charge composition and energy spectra of cosmic-ray nuclei from 3000 MeV per nucleon to 50 GeV per nucleon. Astrophys. J. 223, 676–696. https://doi.org/10.1086/156301.

Lipari, P., 2021. How well do we understand the properties of the Galactic cosmic ray accelerators and of cosmic ray propagation in the Galaxy? A critical view. PoS ICRC2021, 169. https://doi.org/10.22323/1.395.0169.

Marrocchesi, P., Adriani, O., Akaike, Y., et al., 2011. Beam test performance of a scintillator-based detector for the charge identification of relativistic ions. Nucl. Instrum. Methods Phys. Res., Sect. A 659 (1), 477–483. https://doi.org/10.1016/j.nima.2011.08.034, URL: https://www.sciencedirect.com/science/article/pii/S016890021101655X.

Marrocchesi, P.S., 2021. New Results from the first 5 years of CALET observations on the International Space Station. PoS ICRC2021, 010. https://doi.org/10.22323/1.395.0010.

Marrocchesi, P.S., Torii, S., 2019. The CALorimetric Electron Telescope (CALET) on the International Space Station. Adv. Sp. Res. 64 (12), 2531–2537. https://doi.org/10.1016/j.asr.2019.04.013, URL: https://www.sciencedirect.com/science/article/pii/S027311771930273X.

Minagawa, G., 1981. The abundances and energy spectra of cosmic ray iron and nickel at energies from 1 to 10 GeV per AMU. Astrophys J 248, 847–855. https://doi.org/10.1086/159210.

Mueller, D., Swordy, S.P., Meyer, P., et al., 1991. Energy Spectra and Composition of Primary Cosmic Rays. Astrophys. J. 374, 356–365. https://doi.org/10.1086/170125.

Niita, T., Torii, S., Akaike, Y., et al., 2015. Energy calibration of calorimetric electron telescope (calet) in space. Adv. Space Res. 55 (11), 2500–2508. https://doi.org/10.1016/j.asr.2015.03.006, URL: https://www.sciencedirect.com/science/article/pii/S0273117715001891.

Obermeier, A., Ave, M., Boyle, P., et al., 2011. Energy spectra of primary and secondary cosmic-ray nuclei measured with TRACER. Astrophys. J. 742 (1), 14. https://doi.org/10.1088/0004-637X/742/1/14.

Ohira, Y., Kawanaka, N., Ioka, K., 2016. Cosmic-ray hardenings in light of AMS-02 data. Phys. Rev. D 93, 083001. https://doi.org/10.1103/PhysRevD.93.083001, URL: https://link.aps.org/doi/10.1103/PhysRevD.93.083001.

Panov, A.D., Adams, J.H., Ahn, H.S., et al., 2009. Energy spectra of abundant nuclei of primary cosmic rays from the data of ATIC-2 experiment: Final results. Bull. Russ. Acad. Sci.: Phys. 73 (5), 564–567. https://doi.org/10.3103/s1062873809050098, URL: https://doi.org/10.3103%2Fs1062873809050098.

Ptuskin, V., Zirakashvili, V., Seo, E.S., 2013. Spectra of cosmic-ray protons and helium produced in supernova remnants. Astrophys. J. 763, 47. https://doi.org/10.1088/0004-637X/763/1/47.

Serpico, P.D., 2016. Possible physics scenarios behind cosmic-ray anomalies. PoS ICRC2015, 009. https://doi.org/10.22323/1.236.0009.

Thoudam, S., Hörandel, J.R., 2014. GeV-TeV cosmic-ray spectral anomaly as due to reacceleration by weak shocks in the Galaxy. Astron. Astrophys. 567, A33. https://doi.org/10.1051/0004-6361/201322996.

Tomassetti, N., 2012. Origin of the cosmic-ray spectral hardening. Astrophys. J. Lett. 752, L13. https://doi.org/10.1088/2041-8205/752/1/L13.

Vladimirov, A., Johannesson, G., Moskalenko, I., et al., 2012. Testing the origin of high-energy cosmic rays. Astrophys. J. 752, 68. https://doi.org/10.1088/0004-637X/752/1/68.

Yoon, Y.S., Ahn, H.S., Allison, P.S., et al., 2011. Cosmic-ray proton and helium spectra from the first CREAM flight. Astrophys J 728 (2), 122. https://doi.org/10.1088/0004-637X/728/2/122.

Yoon, Y.S., Anderson, T., Barrau, A., et al., 2017. Proton and Helium Spectra from the CREAM-III Flight. Astrophys J 839 (1), 5. https://doi.org/10.3847/1538-4357/aa68e4.

Young, J.S., Freier, P.S., Waddington, C.J., et al., 1981. The elemental and isotopic composition of cosmic rays - Silicon to nickel. Astrophys J 246, 1014–1030. https://doi.org/10.1086/158997.